

UC Riverside

UC Riverside Previously Published Works

Title

Evaluation of Dynamic Cell Processes and Behavior Using Video Bioinformatics Tools

Permalink

<https://escholarship.org/uc/item/8kz4m4sc>

ISBN

9783319237237

Authors

Lin, Sabrina C
Yip, Henry
Phandthong, Rattapol
et al.

Publication Date

2015

DOI

10.1007/978-3-319-23724-4_9

Peer reviewed

Metadata of the chapter that will be visualized in SpringerLink

Book Title	Video Bioinformatics	
Series Title		
Chapter Title	Evaluation of Dynamic Cell Processes and Behavior Using Video Bioinformatics Tools	
Copyright Year	2015	
Copyright HolderName	Springer International Publishing Switzerland	
Author	Family Name	Lin
	Particle	
	Given Name	Sabrina C.
	Prefix	
	Suffix	
	Division	UCR Stem Cell Center, Department of Cell Biology and Neuroscience
	Organization	University of California
	Address	Riverside, 92521, USA
	Email	
Author	Family Name	Yip
	Particle	
	Given Name	Henry
	Prefix	
	Suffix	
	Division	UCR Stem Cell Center, Department of Cell Biology and Neuroscience
	Organization	University of California
	Address	Riverside, 92521, USA
	Email	
Author	Family Name	Phandthong
	Particle	
	Given Name	Rattapol
	Prefix	
	Suffix	
	Division	UCR Stem Cell Center, Department of Cell Biology and Neuroscience
	Organization	University of California
	Address	Riverside, 92521, USA
	Email	
Author	Family Name	Davis
	Particle	
	Given Name	Barbara
	Prefix	
	Suffix	
	Division	UCR Stem Cell Center, Department of Cell Biology and Neuroscience
	Organization	University of California
	Address	Riverside, 92521, USA
	Email	

	Email	
Corresponding Author	Family Name	Talbot
	Particle	
	Given Name	Prue
	Prefix	
	Suffix	
	Division	UCR Stem Cell Center, Department of Cell Biology and Neuroscience
	Organization	University of California
	Address	Riverside, 92521, USA
	Email	talbot@ucr.edu
Abstract	<p>Just as body language can reveal a person's state of well-being, dynamic changes in cell behavior and morphology can be used to monitor processes in cultured cells. This chapter discusses how CL-Quant software, a commercially available video bioinformatics tool, can be used to extract quantitative data on: (1) growth/proliferation, (2) cell and colony migration, (3) reactive oxygen species (ROS) production, and (4) neural differentiation. Protocols created using CL-Quant were used to analyze both single cells and colonies. Time-lapse experiments in which different cell types were subjected to various chemical exposures were done using Nikon BioStations. Proliferation rate was measured in human embryonic stem cell colonies by quantifying colony area (pixels) and in single cells by measuring confluency (pixels). Colony and single cell migration were studied by measuring total displacement (distance between the starting and ending points) and total distance traveled by the colonies/cells. To quantify ROS production, cells were pre-loaded with MitoSOX Red™, a mitochondrial ROS (superoxide) indicator, treated with various chemicals, then total intensity of the red fluorescence was measured in each frame. Lastly, neural stem cells were incubated in differentiation medium for 12 days, and time lapse images were collected daily. Differentiation of neural stem cells was quantified using a protocol that detects young neurons. CL-Quant software can be used to evaluate biological processes in living cells, and the protocols developed in this project can be applied to basic research and toxicological studies, or to monitor quality control in culture facilities.</p>	



Chapter 9

Evaluation of Dynamic Cell Processes and Behavior Using Video Bioinformatics Tools

Sabrina C. Lin, Henry Yip, Rattapol Phandthong, Barbara Davis and Prue Talbot

Abstract Just as body language can reveal a person's state of well-being, dynamic changes in cell behavior and morphology can be used to monitor processes in cultured cells. This chapter discusses how CL-Quant software, a commercially available video bioinformatics tool, can be used to extract quantitative data on: (1) growth/proliferation, (2) cell and colony migration, (3) reactive oxygen species (ROS) production, and (4) neural differentiation. Protocols created using CL-Quant were used to analyze both single cells and colonies. Time-lapse experiments in which different cell types were subjected to various chemical exposures were done using Nikon BioStations. Proliferation rate was measured in human embryonic stem cell colonies by quantifying colony area (pixels) and in single cells by measuring confluency (pixels). Colony and single cell migration were studied by measuring total displacement (distance between the starting and ending points) and total distance traveled by the colonies/cells. To quantify ROS production, cells were pre-loaded with MitoSOX Red™, a mitochondrial ROS (superoxide) indicator, treated with various chemicals, then total intensity of the red fluorescence was measured in each frame. Lastly, neural stem cells were incubated in differentiation medium for 12 days, and time lapse images were collected daily. Differentiation of neural stem cells was quantified using a protocol that detects young neurons. CL-Quant software can be used to evaluate biological processes in living cells, and the protocols developed in this project can be applied to basic research and toxicological studies, or to monitor quality control in culture facilities.

Electronic supplementary material The online version of this article (doi:[10.1007/978-3-319-23724-4_9](https://doi.org/10.1007/978-3-319-23724-4_9)) contains supplementary material, which is available to authorized users.

S.C. Lin · H. Yip · R. Phandthong · B. Davis · P. Talbot (✉)
UCR Stem Cell Center, Department of Cell Biology and Neuroscience,
University of California, Riverside 92521, USA
e-mail: talbot@ucr.edu



9.1 Introduction

Evaluation of dynamic cell processes and behavior is important in basic research [11, 40, 43, 46], in the application of stem cell biology to regenerative medicine [29, 41], and in studies involving the toxicity of drug candidates and environmental chemicals [13, 24, 25, 31, 32, 35–38, 42]. Prior work in basic and toxicological research has often involved microscopic observation of cells or assays that evaluate single endpoints after chemical exposure (e.g., [4, 6–8, 25, 33]). However, much additional insight can be learned about a cells response to its environment by comparing dynamic processes, such as cell growth and motility, in treated and control cells [30, 31, 44]. Just as human body language can reveal information about human mood and well-being, cellular dynamics can often reveal information about the mode of action and the cellular targets of chemical exposure. For example, impairment of cell motility would likely be correlated with an adverse effect on the cytoskeleton. Such an effect can be quantified in video data without using any labels or genetic transformation of the cells [25, 31, 36, 49]. In addition, fluorescent labels can be used to report the condition of cells in time-lapse data thereby revealing more information about a treatment than a single endpoint assay [27]. Finally, multiple endpoints can be multiplexed and mined from video data to gain additional insight from a single experiment [2, 34].

The interest and importance of video data in cellular studies has led to the commercialization of a number of instruments (e.g., BioStation CT/IM, Cell IQ, Tokai Hit) optimized for collecting live cell images over time [10, 44]. Videos can now be made for hours, days, or even months using conditions that support in vitro cell culture and experimentation. However, while dynamic video data are rich with information about cell health and cell processes, they are often difficult to analyze quantitatively. This is due to the complexity of the data and the generally large size of the data sets. Moreover, video analysis can be very time-consuming and is error-prone due to subjectivity of the human(s) performing the analysis. The recent interest in live cell imaging has been accompanied by a need for software tools for extracting information from video data. This field of study has been termed “video bioinformatics” (www.cris.ucr.edu/IGERT/Index.php). Video bioinformatics includes the development and application of software tools for extraction and mining of information and knowledge from video data. The advantages of using video bioinformatics tools are enormous. Tremendous amounts of time can be saved, and when properly applied, video bioinformatics tools will extract more accurate reproducible data than would generally be the case for a human performing the same task. Video bioinformatics tools are available commercially [3] and are also being developed in research laboratories to solve specific problems such as quantification of cells in colonies, cell identification, and prediction of successful development of human embryos to the blastocyst stage [14–17, 21, 51].

In this chapter, four applications of video bioinformatics tools to toxicological problems are presented. First, cell colony and individual cell growth were



monitored using time lapse data. Second, single cell and colony migration were analyzed to provide information on rate of migration, distance traveled, and total displacement. Third, a method is presented for direct observation and quantification of ROS production in cultured cells. Finally, quantification of differentiating neurons was accomplished by evaluating time-lapse videos collected over a period of 10 days. Video data were collected in either a BioStation CT or BioStation IM, both available from Nikon. Analyses were done using protocols created using a commercial software package (CL-Quant). Each application can be used with either single cells or colonies.

9.2 Collection of Time-Lapse Data

The BioStation IM is a fully motorized, automated, environmentally controlled microscope and imaging system that captures images using a cooled monochrome CCD camera. It was designed to enable live cell imaging using optimal in vitro conditions. It can accommodate 35 mm culture dishes including HiQ4 dishes (Nikon Instruments Inc., Melville, NY) that allow four different treatments to be monitored in a single experiment. Cells are incubated at 37 °C in a CO₂ controllable atmosphere with a high relative humidity. Multiple magnifications are possible for capturing phase contrast and/or fluorescence images using software that controls point selection and collection of data. Perfusion is an option to allow for real-time addition or subtraction of cell culture media and to enable longer-term observation. The BioStation IM robotics are capable of precise cell registration so the resultant movies can be analyzed quantitatively.

The BioStation CT is a much larger incubation unit that can perform high content work ideal for live cell screening. The culture conditions inside the BioStation CT can be regulated. While our unit is usually operated at 5 % CO₂, 85 % relative humidity and 37 °C, hypoxic conditions are also possible if needed. The BioStation CT is especially suitable for data collection in long-term experiments, in which cells are studied over weeks or months. It has a robotic arm for transfer of plates to and from a microscope stage which enables complete automation of the time-lapse experiment. The BioStation CT holds up to 30 experimental samples in various plate formats (6, 12, 24, 48, 96 well plate formats, 35, 60 and 100 mm dish formats, and 25 and 75 cm² flask formats). A cooled monochrome CCD camera collects phase and/or fluorescence images at defined intervals and points of interests. Large montages of the entire well area can be taken over the magnification range of 2×–40× which allows for complete cell characterization over the life of the cell culturing period.



9.3 CL-Quant Software

All video analyses were performed using CL-Quant software, a live-cell image analysis program produced for Nikon by DRVision Technologies (Bellevue, Washington). It can either be purchased from Nikon as CL-Quant or from DRVision under the name SVCCell. The current version of the software is user friendly, features an intuitive GUI to manage high content imaging experiments, and comes with webinar instruction. All ground-truth evaluations of CL-Quant were done using either ImageJ or Photoshop.

CL-Quant comes with several modules professionally developed by DRVision for basic processing of videos. For example, bioinformatics tools for measuring cell confluency, cell migration, and cell counting can be obtained from Nikon and applied to users' videos. CL-Quant also provides tools that end users can work with to develop protocols for recognition and quantitative analysis of microscopic video data [3]. CL-Quant protocols can be applied with user directed learning and do not require image processing knowledge. Although the software has great depth, basic analyses can be done with relatively little training. CL-Quant can be used to detect, segment, measure, classify, analyze, and discover cellular phenotypes in video data. Preconfigured modules are available for some applications such as cell counting, confluency, cell division, wound healing, cell motility, cell tracking, and measuring neurite outgrowths. Moreover, the software has significant depth and can be configured for other more complex applications by the user.

In this chapter, examples will be shown for adapting CL-Quant to measure cell/colony growth rate, cell/colony migration, ROS production, and neural differentiation. Protocols, developed by DRVision and Nikon software engineers and those created by novices learning to use the CL-Quant software, will be compared and used to study cell behavior. The above parameters can be useful in toxicological studies, in work that requires knowledge of cell health, in clinical applications of stem cells to regenerative medicine, or in basic studies of cell biology.

9.4 Cell and Colony Growth

9.4.1 Growth of Human Induced Pluripotent Stem Cells (hiPSC)

Human-induced pluripotent stem cells (hiPSC; RivCAG-GFP), created in the UCR Stem Cell Core Facility and grown in 12-well plates as described previously [28] were either incubated in control medium (mTeSR, Stem Cell Technologies) or in mTeSR containing 0.1 puff equivalents (PE) of sidestream cigarette smoke (PE = the amount of smoke in one puff that dissolves in 1 ml). This concentration was shown previously to inhibit human embryonic stem cells (hESC) colony growth [31]. Cells were imaged at 10 \times magnification for 48 at 6 h intervals in a



BioStation CT maintained at 37 °C, 5 % CO₂ and a relative humidity of 85–90 %. Phase contrast images show the growth of a single control and treated colony over 48 h (Fig. 9.1a–c and g–i). All colonies analyzed were selected to be relatively close in size before treatment. During incubation, the sizes of the treated colonies appeared to be smaller than the control colonies. Some treated colonies did not grow, and some eventually died due to treatment (as shown in Fig. 9.1i). To obtain quantitative information on colony growth rates, a protocol, which was developed in our lab with the CL-Quant software (version 3.0) and used previously with hESC [31], was applied to these iPSC video data. The protocol first segmented images of control and treated colonies and overlaid each colony with a mask (Fig. 9.1d–f and j–l). The fidelity of the mask was excellent for both control and treated groups. After images were segmented, small objects, dead cells, and debris were removed with an enhancement module, and finally the size of each colony was measured in pixels in each frame of each video. Because each colony is slightly different at the start of an experiment, resulting data for each set of videos were normalized to the size of the colony in frame 1, then data were averaged and growth curves were graphed (Fig. 9.1m). Results showed a clear difference in growth rates between the control and treated colonies. In fact, the treated colonies decreased in size and appeared not to grow over the 48 h incubation period. Treatment was significantly different than the control (2-way ANOVA, $p \leq 0.05$), and the iPSC were more sensitive to sidestream smoke treatment than the hESC studied previously [32]. The protocol used for this analysis had previously been compared to ground-truth derived using Adobe Photoshop, and excellent agreement was found between the data obtained with CL-Quant analysis and the ground-truth [31].

The data shown in Fig. 9.1 involved analysis of 60 images. To perform this analysis by hand would require approximately 3–4 h. CL-Quant was able to perform this analysis in about 1 h, and it can be run in a large batch so that the users' time is not occupied during processing. With a larger experiment having more frames, the difference between CL-Quant and manual analysis would be much greater.

Video examples of iPSC colony growth and CL-Quant masking can be viewed by scanning the bar code.

9.4.2 Growth of Mouse Neural Stem Cells (mNSC)

Monitoring the growth of single cells can be more challenging than monitoring hiPSC or hESC colony growth. Some single adherent cells grow very flat and do not differ much in contrast from the background making segmentation difficult. However, images can be enhanced by adjusting the brightness, the contrast, and/or the gamma parameters using CL-Quant software or other image processing software (e.g., Photoshop and ImageJ). CL-Quant comes with some professionally developed modules for use with some types of single cells. Investigators can try these protocols to see if one works well with their cell type or, alternatively, they

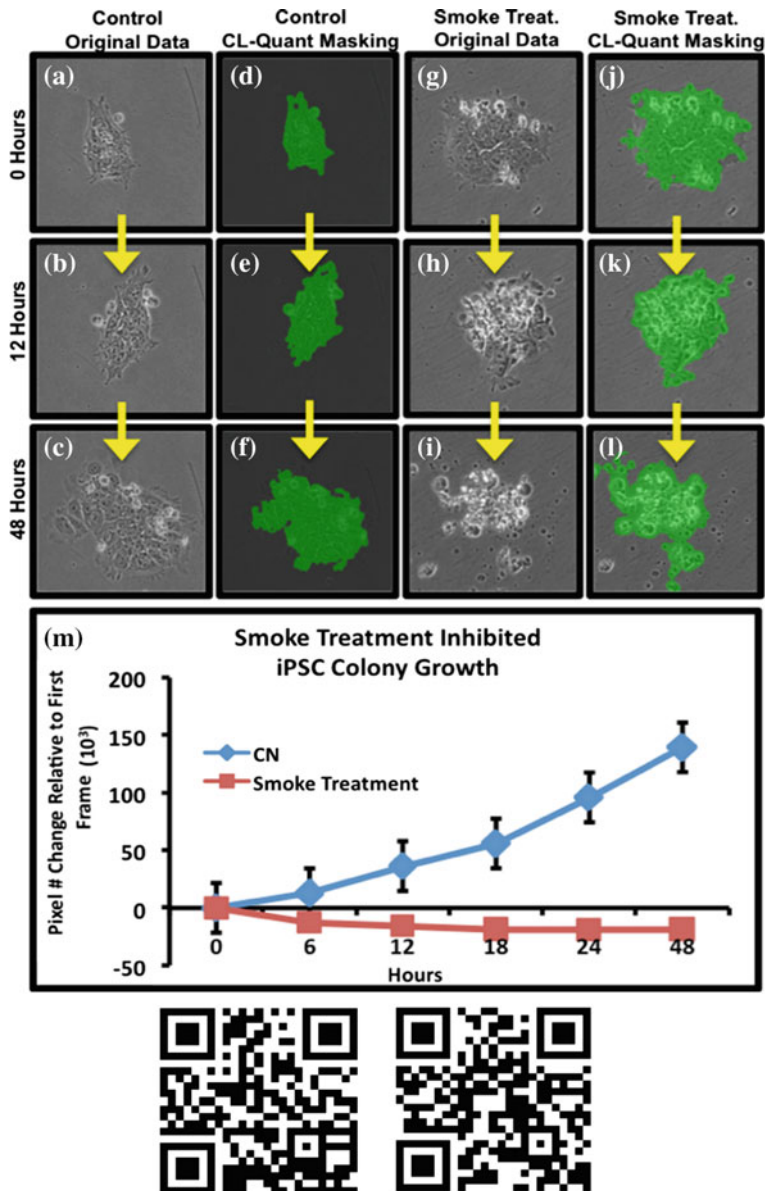


Fig. 9.1 Growth of hiPSC colonies over 48 h. **a–c** Phase contrast images of control iPSC colonies at various times during growth. **d–f** The same control images segmented using a CL-Quant protocol developed in our lab. **g–i** Phase contrast images of smoke treated iPSC colonies at various times during growth. **j–l** The same treatment group images masked using the same CL-Quant protocol as applied to control colonies. **m** Graph of control and treated cells showing growth rate. Data are means and standard errors of three experiments. *CN* control

can use the CL-Quant software to develop their own protocol and tailor it to the specific requirements of the cells they are using. However, one should not assume that the protocols are accurate and should check them against ground-truth.

In our experiments, the effect of cigarette smoke treatment on mNSC proliferation was examined. mNSC were plated in 12-well plates at 2,500 cells/well, and cells were allowed to attach for 24 h before treatment, incubation, and imaging. Various fields of interests were imaged over 48 h in the BioStation CT in 5 % CO₂ and 37 °C. The collected video data (Fig. 9.2a–c) were then processed and analyzed

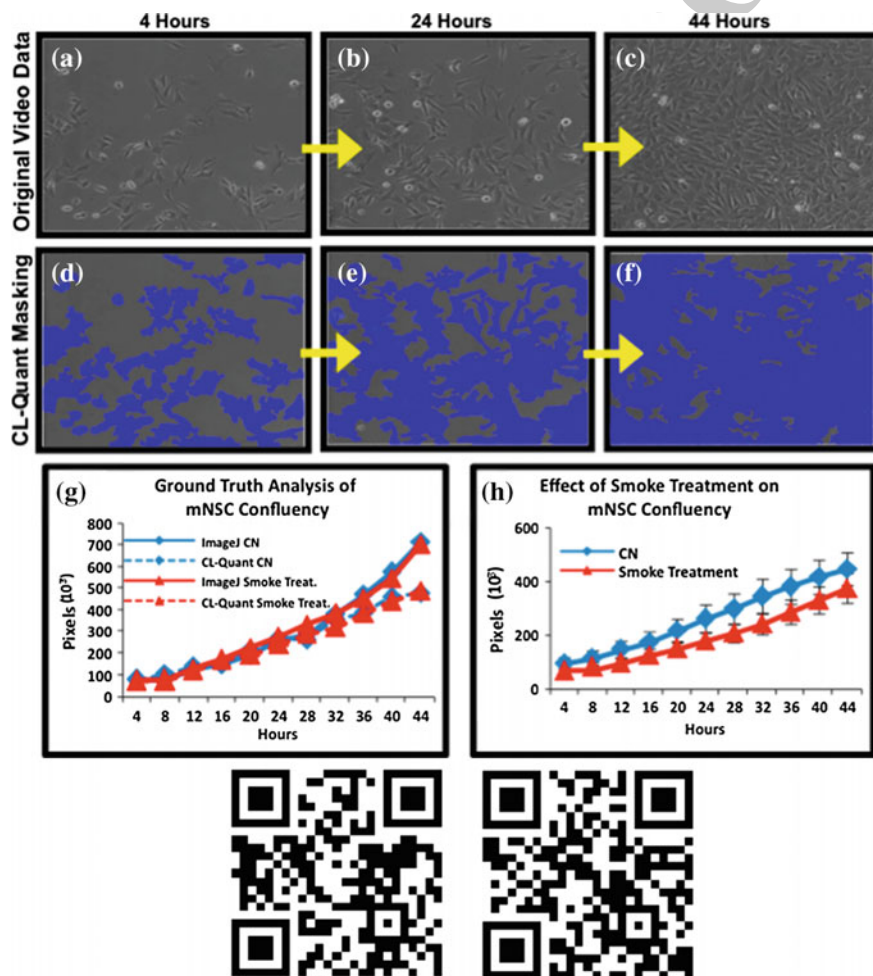


Fig. 9.2 Growth of single mNSC. **a–c** Phase contrast images of control mNSC at various times during growth over 48 h. **d–f** The same images after segmentation using a protocol developed by DR Vision. **g** Graph showing analysis for growth rate of control and treated cells (*solid lines*) and ImageJ ground-truth for each group (*dotted lines*). **h** Graph of control and treated mNSC showing confluency rate. Data are means and standard errors of three experiments. *CN* control



using the confluency module provided by DRVision Technologies for use with CL-Quant software. The confluency module masked the cells in each field, and mNSC growth was determined by measuring the number of pixels in each frame (Fig. 9.2d–f). Ground-truth was obtained to verify the validity of the CL-Quant confluency analysis tool using ImageJ. To obtain ground-truth, each cell was carefully outlined and colored to measure area (pixels), and a comparison of CL-Quant and ImageJ data showed CL-Quant was reliable over the first 34 h with some divergence at the latest times (Fig. 9.2g). A complete mNSC growth experiment was analyzed in which the growth of cigarette smoke treated cells was compared to nontreated control cells (Fig. 9.2h). Smoke treatment of mNSC significantly inhibited their proliferation from 20 to 44 h (2-way ANOVA, $p \leq 0.001$).

Video examples of mNSC proliferation (control and smoke treatment) can be viewed by scanning the bar code.

9.5 Cell Migration

9.5.1 Migration of hESC Colonies

Evaluation of cell motility can be important in determining if the cytoskeleton of treated cells has been affected. The data in Fig. 9.3 were collected using hESC colonies that were incubated in a BioStation CT for 48 h, and images were collected of each colony at 10 min intervals. Colonies, which were grown on Matrigel, were incubated in either control medium (mTeSR) or mTeSR containing cigarette smoke. Normally, hESC show motility when grown on a Matrigel.

CL-Quant provides a number of readouts for motility. The two that were most useful are total distance traveled and total displacement. Total distance traveled is the measurement of how far the colony has migrated over time, and total displacement is the difference in distance between the beginning point and the end-point. Figure 9.3a–c shows examples of hESC colonies that have been masked and tracked by a motility protocol. Within a population of hESC colonies, three behaviors were observed: (1) growing, (2) shrinking, and (3) dying. The tracking module traces the path of the colonies, and those that showed growth had longer paths than colonies that were shrinking or dying.

In Fig. 9.3d, e, displacement and total distance traveled were measured for individual colonies in control and cigarette smoke treatment groups. All colonies in the control group were healthy and growing, but 2 of 12 treated colonies (red circles) were dead by the end of 48 h. For total distance traveled, measurements for control colonies appeared to be clustered, while the treated colonies were more variable, in part due to the presence of two dead colonies. For both the control and treated groups, the total displacement was quite variable, suggesting there was no directional movement in either group. A t test was performed on both parameters, after removing measurements of dying colonies, and the results showed that the

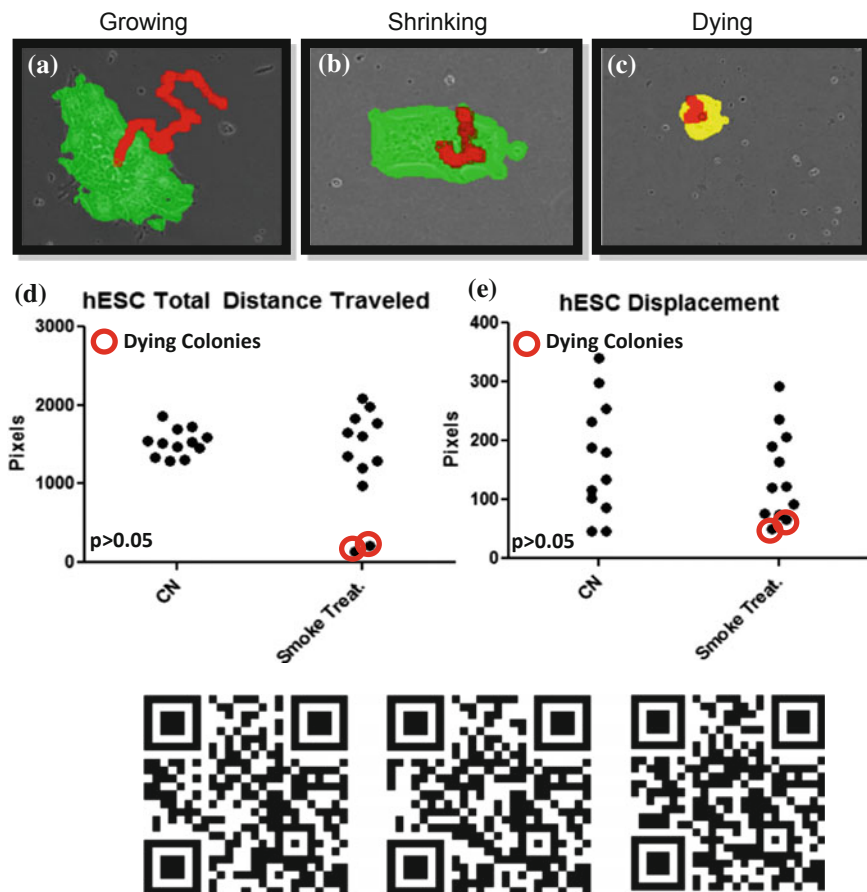


Fig. 9.3 Migration of hESC colonies. **a** Masked phase contrast image of a growing hESC colony during migration. **b** Masked phase contrast image of a shrinking hESC colony during migration. **c** Masked phase contrast image of a dying hESC colony during migration. **d, e** Graphs showing total displacement/distance traveled for each control and treated colonies. All CL-Quant masking and tracking of colonies were done by applying a tracking recipe developed by our lab. *CN* control

distance traveled and displacement of control and treated colonies were not significantly different ($p > 0.05$).

hESC migration is an important process during development, as derivatives of these cells must migrate during gastrulation to form the three germ layers properly [22]. Therefore, although our cigarette smoke treatment did not affect migration of hESC colonies, these two parameters can be useful in determining the effects of other toxicants on pluripotent cell migration. Observed effects on total distance traveled and displacement of colonies can be the first signs of potent chemical effects on the cytoskeletal integrity of the cells.

Video examples of hESC colony migration and CL-Quant masking can be viewed by scanning the bar codes.

9.5.2 Migration and Gap Closure of mNSC and NTERA2 Cells

Single cell migration can be analyzed using a gap closure assay. This assay is performed by growing a monolayer of cells, creating a gap in the middle of the monolayer, and monitoring the time required for cells to migrate into the gap and close it. The gap can be made using a pipette to remove a band of cells, but the sizes of the gaps are not always uniform. As a result, the rate of closure may not be as accurate and comparable among control and treated groups. We have used Ibidi wound healing culture inserts (Fig. 9.4, Ibidi, cat#80241, Verona, WI) to make uniform gaps. First, inserts were adhered to culture plates. Second, cells were plated in each well of the insert, and when cells in the wells were confluent, the insert was removed leaving a uniform gap (500 μm) between cells in each well. This method works well with cells grown on plastic or glass, but not with cells grown on wet coating substrates (e.g., Matrigel, poly-D-lysine, poly-L-lysine, and laminin) because the adhesive at the bottom of the inserts will not stick.

Experiments using two types of cells, mNSC and NTERA2, are shown in Fig. 9.5. Both cell types can be grown on plastic, and time-lapse videos of both cell types were collected in the BioStation CT for 44 h. Images were collected every 4 h and CL-Quant analysis was done for each frame by measuring the number of pixels in the gap. The gap closure module, developed by our lab using the CL-Quant software, includes a segmentation recipe to identify the gap between the two populations of cells and a measurement recipe that counts the number of pixels in the gap. An example of mNSC gap closure images is shown in Fig. 9.5a–c, and CL-Quant masking of the same gap is shown in Fig. 9.5d–f. In the filmstrip, the gap became smaller as the cells migrated toward each other. Gap closure analysis using the CL-Quant software was validated using ground-truth obtained from the ImageJ software for control and treated NTERA2 (Fig. 9.5g, h). While CL-Quant tended to

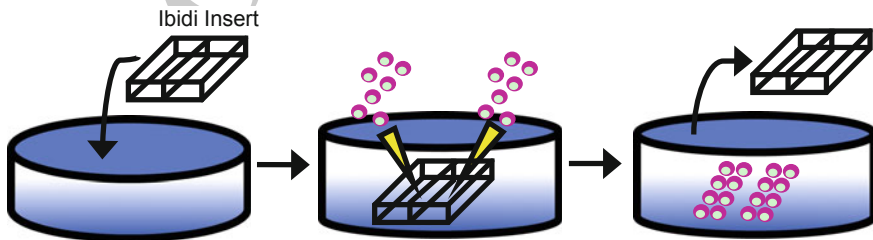
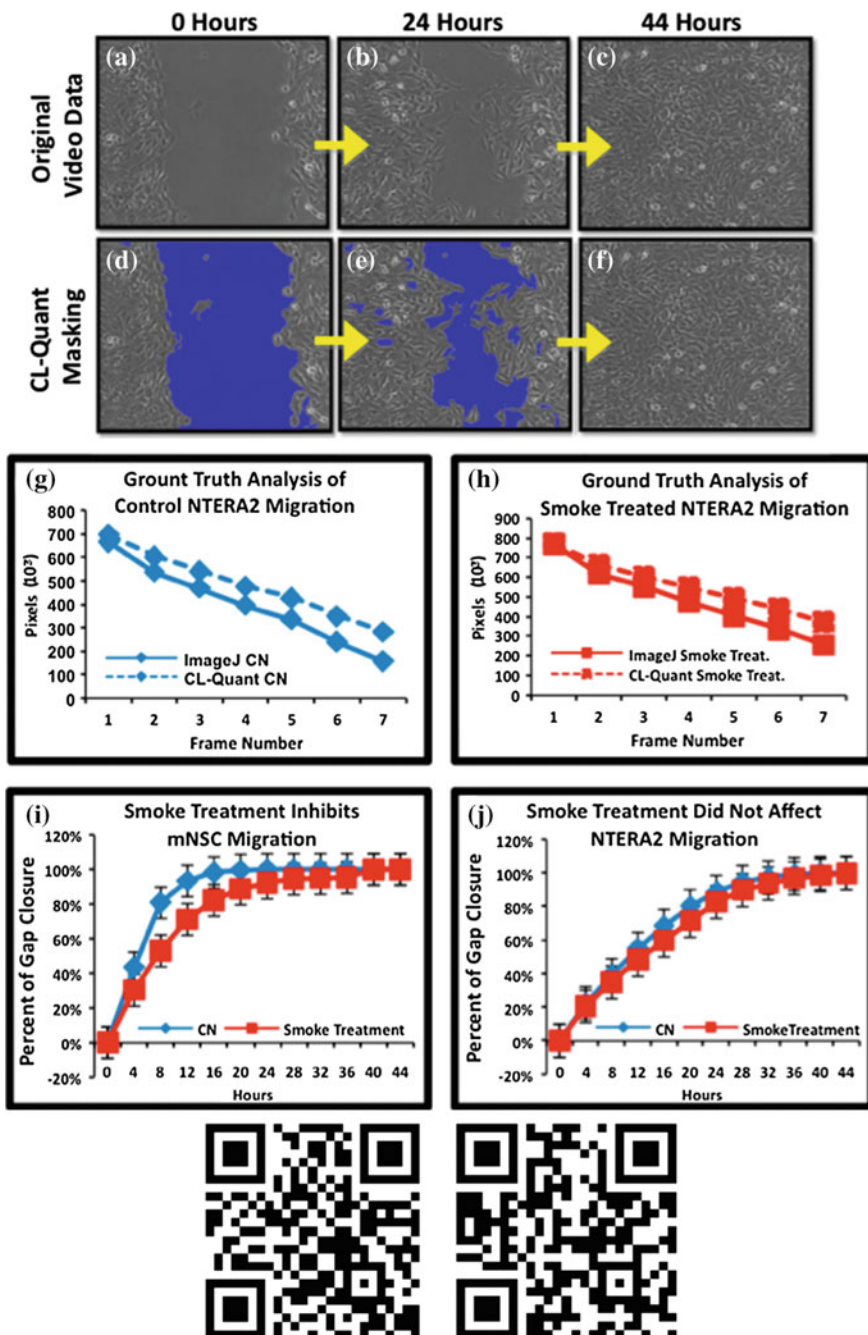


Fig. 9.4 Diagram of Ibidi gap closure culture inserts



◀ **Fig. 9.5** Gap closure for mNSC and NTERA2 cells. **a–c** Phase contrast images of mNSC at various 3 times during gap closure. **d–f** The same images after segmentation using a protocol developed in our lab with CL-Quant software. **g, h** Graph showing rate of gap closure for control (blue) and treated NTERA2 cells (red) and the corresponding ground-truth (dotted lines) obtained using ImageJ. **i** Graph of mNSC migration by monitoring percent of gap closure over 44 h. **j** Graph of NTERA2 cell migration by monitoring percent of gap closure over 44 h. Data are means and standard errors of three experiments

overestimate area slightly due to some extension of the mask beyond the gap, ImageJ and CL-Quant analyses produced similar results for both control and treated groups. mNSC and NTERA2 cell migration experiments were analyzed with the CL-Quant gap closure module (Fig. 9.5i, j). Gap closure was completed in about 16 h for the mNSC, while the NTERA2 cells required about 40 h to completely close the gap. Migration of mNSC, but not the NTERA2, was significantly inhibited by cigarette smoke ($p \leq 0.001$ for 2-way ANOVA of mNSC data).

Although our gap closure analysis was done by measuring the pixels within the gap, it can also be monitored by masking the cells. For certain cells that produce a clear phase contrast image, this option may be easier and more accurate than monitoring the gap.

Video examples of control and smoke treated single cell migration can be viewed by scanning the bar codes.

9.6 Detection of Reactive Oxygen Species (ROS) in Human Pulmonary Fibroblasts (HPF)

Exposure to environmental chemicals can lead to stress [9, 12, 26, 47], and ROS are often produced in stressed cells [1, 19, 45]. ROS can damage macromolecules in cells including proteins and DNA, and any factor that increases ROS would be potentially damaging to a cell. It is possible to observe the production of ROS in cells using fluorescent probes such as MitoSOX Red™ (Life Technologies, Grand Island, NY). MitoSOX Red™ readily enters cells and is rapidly targeted to the mitochondria. When oxidized by superoxide, it emits red fluorescence (absorption/emission maxima = 510/580). MitoSOX Red™ can be preloaded in cells and will fluoresce as levels of superoxide increase. Its fluorescent intensity is related to the amount of superoxide in the cells.

In this example, hPF were disassociated from a culture vessel using 0.05 % trypsin and then plated in the HiQ4 dishes coated with poly-D-lysine. After hPF were allowed to attach for 24 h, cells were preloaded with 5 μ M MitoSOX Red™ for 10 min at 37 °C in a cell culture incubator. Preloaded cells were washed with culture medium and then either treated with cigarette smoke which induces ROS production [47] or were left untreated (control). Dishes were placed in a BioStation IM, which was programmed to capture images every 4 min for 10 h using both the phase and red fluorescence channels.

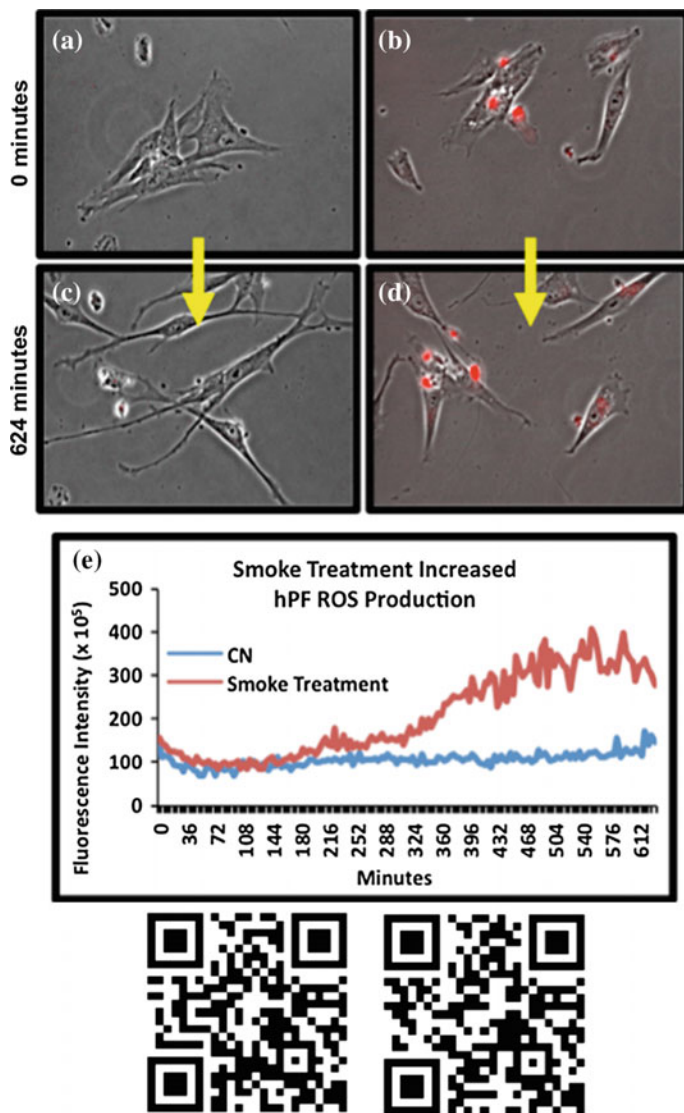


Fig. 9.6 Production of reactive oxygen species in hPF. **a–d** Merged phase contrast and fluorescent images at various times during incubation of control and treated hPF with MitoSox Red. **e** Graph showing fluorescence intensity in control and treated cells over time. *CN* control

A protocol was developed using CL-Quant to analyze the level of MitoSOX RedTM fluorescence in living cells. This was done by first developing a segmentation procedure to identify fluorescence. An enhancement program was then used to remove all debris and dead cells. The dead cells are highly fluorescent but round and easily excluded from the analysis with a size-based enhancement filter.



The background was flattened, and the mask was applied and observed to determine if it accurately covered each cell in the entire video. If the mask was not accurate, the segmentation was refined until masking accurately covered all living cells in each frame. CL-Quant was then used to measure the level of fluorescence in each field of each video.

The above protocol was applied to time-lapse videos of control and cigarette smoke treated hPF that were preloaded with MitoSOX Red™. Merged phase contrast and fluorescent images of control and treated cells are shown at various times in Fig. 9.6a–d. There are usually some highly fluorescent dead cells present in each field at the start of an experiment. It is important to filter out the dead cells before performing the analysis as they would contribute significantly to the intensity measurements. The graph shows the intensity of the MitoSOX Red™ fluorescence in control and treated cells over 10 h of incubation (Fig. 9.6e). Control levels remained low and relatively constant throughout incubation in agreement with direct observation of the videos. In contrast, fluorescence increased significantly in the treated cells. This increase begins at about 300 min of incubation and continues until the end of the experiment. This method is useful for direct monitoring of ROS production in time-lapse images. It reports which cells produce ROS, the relative amounts of ROS in control and treated groups, and the time at which ROS is elevated. Statistical analysis showed that cigarette smoke treatment significantly increased hPF ROS production over time (2-way ANOVA, $p \leq 0.001$).

Video examples of hPF ROS production in control and treated cells can be viewed by scanning the bar codes.

9.7 Detection and Quantification of Spontaneous Neural Differentiation

Differentiation of stem cell populations is an essential and important process of normal development. Many in vitro differentiation protocols have been established to derive various cell types that can then be used for degenerative disease therapy, organ regeneration, and models for drug testing and toxicology research [42]. In all cases, the health, morphology, and differentiation efficiency of the cells are important parameters that should be closely observed and evaluated. Here, we provide an example of how differentiating mNSC are monitored over time and derived neurons are quantified using the CL-Quant software. mNSC were plated in 12-well plates in NeuroCult™ Differentiation Medium (Stem Cell Technologies, Vancouver, Canada) for 12 days. The plate was incubated in the Nikon BioStation CT, and several fields of interest were randomly chosen for imaging every 24 h. The NeuroCult™ Differentiation Medium supports the differentiation of three brain cell types: (1) neurons, (2) astrocytes, and (3) oligodendrocytes. The morphologies of these three cell types are very different in that neurons have long axons and small cell bodies, and astrocytes and oligodendrocytes are flatter in appearance. As seen

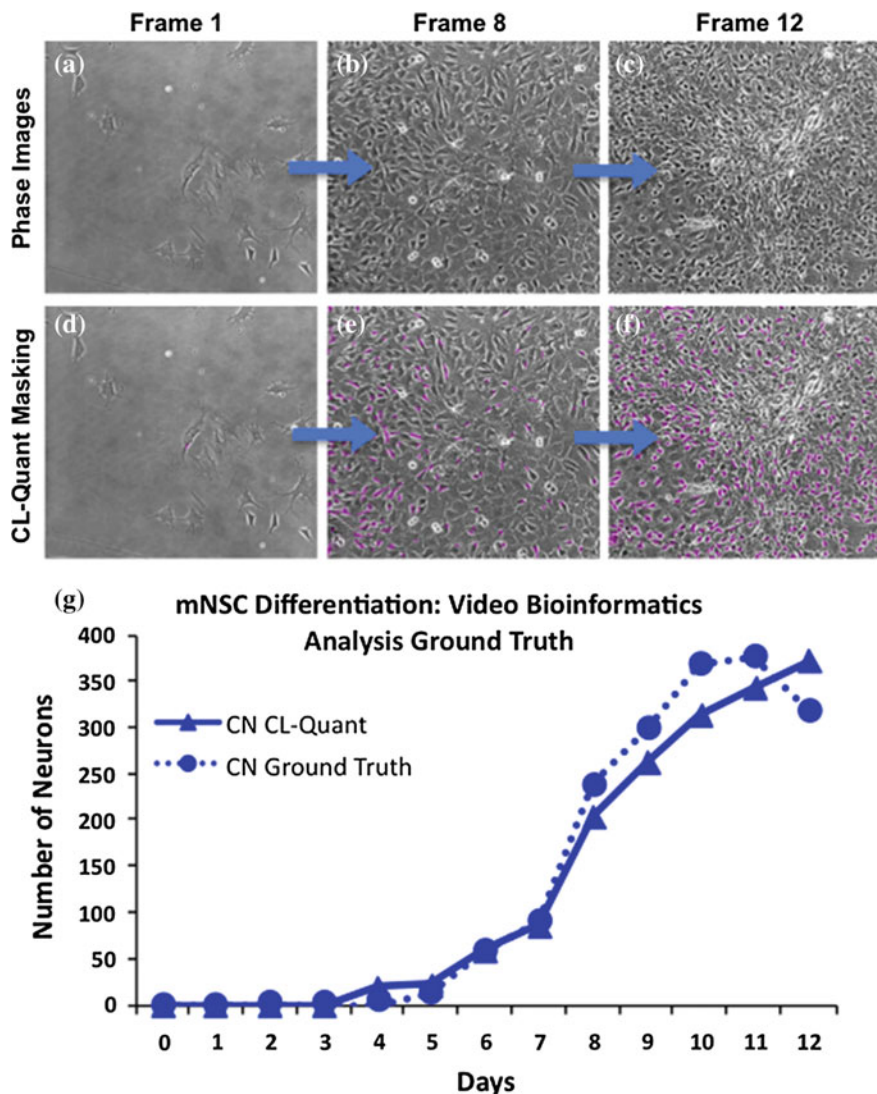


Fig. 9.7 Quantification of neurons in neural differentiation assay. **a–c** Phase contrast images of mNSC at various times during incubation. **d–f** CL-Quant software masking of mNSC phase contrast images to identify the neurons within each frame. **g** Graph showing quantification results obtained using the CL-Quant software was similar to the ground-truth obtained using the ImageJ software

in Fig. 9.7a–c, phase contrast microscopy of the differentiating neural stem cell population showed small, dark neurons sitting on top of a layer of flat cells. The stark morphological differences can be used to quantify the number of neurons in each frame. A segmentation recipe was developed using the CL-Quant software to



identify the darker and smaller neurons (Fig. 9.7d–f), and a measurement recipe was used to count the number of neurons in each frame. We further validated our recipe with ground-truth generated using the ImageJ software (Fig. 9.7g), and the number of neurons identified in each frame using the video bioinformatics tool agreed closely to the ground-truth data. Automation of the identification process is a critical component for making future stem cell research more efficient and effective.

9.8 Discussion

This chapter gives four examples of how video bioinformatics tools can be applied to experimental time-lapse data thereby enabling quantification of dynamic cellular processes with attached cells that grow as colonies or single cells. Live cell imaging is easily obtainable with modern instrumentation designed for culturing cells in incubators equipped with microscopes [44]. Analysis of such data, as shown above, can be done using professionally developed software tools [3] or tools developed by end users with software such as CL-Quant [31, 44, 49]. However, any commercial software may be limited in its ability to segment difficult subjects, in which case custom software would need to be created [14–16, 21, 51]. In all of the examples mentioned, use of video bioinformatics tools significantly reduced the time for analysis and provided greater reproducibility than would normally be obtained with manual human analysis. Although not demonstrated in this chapter, the power of live cell imaging can be increased by multiplexing several endpoints together in one experiment. For example, hESC or iPSC colony growth and migration can be evaluated from the same set of video data, thereby conserving time and resources.

We demonstrated how video bioinformatics tools were used to evaluate the effects of cigarette smoke on dynamic processes (growth, migration, and ROS production) in cultured cells. Many *in vitro* toxicological assays (e.g., MTT, neutral red, and lactic dehydrogenase assays) are useful and effective in evaluating chemical potency. Several recent studies from our lab effectively used the MTT assay to screen the toxicity of various electronic cigarette fluids with embryonic stem cells, mNSC, and hPF [4, 6, 7, 50]. Due to the sensitive nature of hESC cultures, a new 96-well plate MTT protocol was also established for pluripotent cells, which allows exact numbers of cells (in small clumps) to be plated from well to well [6, 7]. While these *in vitro* assays are relatively quick and efficient, they provide a single endpoint at one time/experiment, and the cells are often killed to obtain the endpoint. As a result, dynamic changes in cell behavior and morphology are not observed, and potential data are lost. In both basic research and toxicological applications, examination of video data can reveal changes in cell dynamics as well as rate data that are not gathered by single time point analysis. By determining specific processes that are altered during treatment, the mode of action and cellular targets may be identified. As an example, motility of mNSC, but not of NTERT-2 cells, was affected by cigarette smoke, suggesting that the cytoskeleton is



more sensitive to smoke exposure in the former cells. Observations made from time-lapse video data also provide insight on when during exposure chemicals affect dynamic cellular processes.

Although this chapter presented toxicological applications of video bioinformatics tools, other biological disciplines can benefit from this approach. For example, Auxogyn, Inc. has established a method to determine the health of early human embryos using time-lapse microscopy and an automated embryo stage classification procedure [48, 51]. The protocol employs a set of learned embryo features that allow 88 % classification accuracy of embryos that will develop to the blastocyst stage. This advancement is being used in in vitro fertilization (IVF) clinics to help physicians transfer only healthy embryos with the capacity to develop into blastocysts. This not only increases IVF success rates, but decreases the chance for multiple births that often result in unhealthy children. In June 2013, Auxogyn announced the birth of the first baby to be born in an IVF clinic that used the “Early Embryo Viability Assessment” (Eeva) test to select the best embryos for transfer (<http://www.auxogyn.com/news.2013-06-14.first-auxogyn-baby-born-in-scotland.php>).

The use of video bioinformatics tools will also be important when monitoring the health of cells that will eventually be used in stem cell therapy. In the future, stem cells grown for transfer to patients will be cultured over long periods during passaging and differentiation making them costly in time and resources. Therefore, it is important to monitor the culturing process using time-lapse data to verify that cells are healthy and robust throughout in vitro culture and differentiation. It will be important to have noninvasive monitoring systems for stem cell applications in regenerative medicine. If a problem develops during expansion and culturing of cells used in therapy, experiments can be terminated and restarted to assure that only cells of excellent quality are transferred to patients.

Time-lapse data are also used in basic studies of cell biology. Qualitative and quantitative analysis of video data have revealed information on dynamic cellular processes [18, 20, 27], such as spindle formation during mitosis, actin protein dynamics in cells, and gamete fusion [5, 23, 39]. Video data can also be used to study cell processes that occur rapidly and are not easily understood by direct observation, such as the acrosome reaction of lobster sperm [46]. Frame-by-frame analysis of the acrosome reaction enabled each step during acrosomal eversion to be analyzed and further enabled quantitative measurement of the forward movement of sperm during the reaction. Time-lapse video microscopy has also been used to study the process and rate of oocyte cumulus complexes pick-up by explants of hamster oviducts [43].

New instrumentation, such as the Nikon BioStation CT/IM, provide long-term stable incubation conditions for live cell imaging and enable acquisition of better quality data than possible in the past. Improved methods for live cell imaging coupled with video bioinformatics tools provide a new technology applicable to numerous fields in the life sciences.



Acknowledgments Work presented in this chapter was supported by the following grants: TRDRP 22RT-0127, CIRM NE-A0005A-1E, NSF IGERT DGE 093667, a Cornelius Hopper Award from TRDRP, and a TRDRP postdoctoral fellowship 20FT-0084. We thank Dr. Evan Snyder for providing the mNSC and Randy Myers and Ned Jastromb for their help with the BioStations and CL-Quant.

References

1. Adler V, Yin Z, Tew KD, Ronai Z (1999) Role of redox potential and reactive oxygen species in stress signaling. *Oncogene* 18:6104–6111
2. Albrecht DR, Underhill GH, Resnikoff J, Mendelson A, Bhatiaacde SN, Shah JV (2010) Microfluidics-integrated time-lapse imaging for analysis of cellular dynamics. *Integr Biol* 2:278–287
3. Alworth SV, Watanabe H, Lee JS (2010) Teachable, high-content analytics for live-cell, phase contrast movies. *J Biomol Screen* 15(8):968–977. 1087057110373546 [pii]
4. Bahl V, Lin S, Xu N, Davis B, Wang Y, Talbot P (2012) Comparison of electronic cigarette refill fluid cytotoxicity using embryonic and adult models. *Reprod Toxicol* 34(4):529–537. doi:10.1016/j.reprotox.2012.08.001
5. Ballestrem C, Wehrle-Haller B, Imhof BA (1998) Actin dynamics in living mammalian cells. *J Cell Sci* 111:1649–1658
6. Behar RZ, Bahl V, Wang Y, Weng J, Lin SC, Talbot P (2012) Adaptation of stem cells to 96-Well plate assays: use of human embryonic and mouse neural stem cells in the MTT assay. *Curr Protoc Stem Cell Biol Chapter 1: Unit1C 13*
7. Behar RZ, Bahl V, Wang Y, Lin S, Xu N, Davis B, Talbot P (2012) A method for rapid dose-response screening of environmental chemicals using human embryonic stem cells. *J Pharmacol Toxicol Methods* 66:238–245. doi:10.1016/j.vascn.2012.07.003
8. Behar RZ, Davis B, Wang Y, Bahl V, Lin S, Talbot P (2013) Identification of toxicants in cinnamon-flavored electronic cigarette refill fluids. *Toxicol In Vitro*. doi:10.1016/j.tiv.2013.10.006
9. Carlson C, Hussain SM, Schrand AM, Braydich-Stolle LK, Hess KL, Jones RL, Schlager JJ (2008) Unique cellular interaction of silver nanoparticles: size-dependent generation of reactive oxygen species. *J Phys Chem* 112:13608–13619
10. Cervinka M, Cervinkova Z, Rudolf E (2008) The role of time-lapse fluorescent microscopy in the characterization of toxic effects in cell populations cultivated in vitro. *Toxicol In Vitro* 22(5):1382–1386. doi:10.1016/j.tiv.2008.03.011. S0887-2333(08)00082-9 [pii]
11. DiCarantonio G, Shaoulia R, Knoll M, Magers T, Talbot P (1995) Analysis of ciliary beat frequencies in hamster oviductal explants. *J Exp Zool* 272(2):142–152
12. Drechsel DA, Patel M (2008) Role of reactive oxygen species in the neurotoxicity of environmental agents implicated in Parkinson's disease. *Free Radic Biol Med* 44:1873–1886
13. Gieseke C, Talbot P (2005) Cigarette smoke inhibits hamster oocyte pickup by increasing adhesion between the oocyte cumulus complex and oviductal cilia. *Biol Reprod* 73(3):443–451
14. Guan BX, Bhanu B, Thakoor N, Talbot P, Lin S (2011) Human embryonic stem cell detection by spatial information and mixture of Gaussians. In: IEEE first international conference on healthcare informatics, imaging and systems biology, pp 307–314
15. Guan BX, Bhanu B, Talbot P, Lin S (2012) Detection of non-dynamic blebbing single unattached human embryonic stem cells. In: International conference on image processing. IEEE, pp 2293–2296
16. Guan BX, Bhanu B, Thakoor NS, Talbot P, Lin S (2013) Automatic cell region detection by k-means with weighted entropy. In: 10th international symposium biomedical imaging (ISBI). IEEE, pp 418–421



17. Guan BX, Bhanu B, Talbot P, Lin S (2014) Bio-driven cell region detection in human embryonic stem cell assay. *IEEE/ACM Trans Comput Biol Bioinform* 11(3):604–611. doi:10.1109/TCBB.2014.2306836
18. Haraguchi T (2002) Live cell imaging: approaches for studying protein dynamics in living cells. *Cell Struct Funct* 27:333–334
19. Held P (2010) An introduction to reactive oxygen species. *BioTek Application Guide*. <http://www.biotech.com/resources/articles/reactive-oxygen-species.html>
20. Hinchcliffe E (2005) Using long-term time-lapse imaging of mammalian cell cycle progression for laboratory instruction and analysis. *Cell Biol Educ* 4:284–290
21. Huth J, Buchholz M, Kraus JM, Schmucker M, Wichert GV, Krndija D, Seufferlein T, Gress TM, Kestler HA (2010) Significantly improved precision of cell migration analysis in time-lapse video microscopy through use of a fully automated tracking system. *Biomed Central Cell Biol* 11:24. <http://www.biomedcentral.com/1471-2121/11/24>
22. Ichikawa T, Nakazato K, Keller PJ, Kajiura-Kobayashi H, Stelzer EHK, Mochizuki A, Nonaka S (2013) Live imaging of whole mouse embryos during gastrulation: migration analyses of epiblast and mesodermal cells. *PLoS One* 8(7):e64506. doi:10.1371/journal.pone.0064506
23. Inoué S, Oldenbourg R (1998) Microtubule dynamics in mitotic spindle displayed by polarized light microscopy. *Mol Biol Cell* 9:1603–1607
24. Knoll M, Talbot P (1998) Cigarette smoke inhibits oocyte cumulus complex pickup by the oviduct in vitro independent of ciliary beat frequency. *Reprod Toxicol* 12(1):57–68
25. Knoll M, Shaoulain R, Magers T, Talbot P (1995) Ciliary beat frequency of hamster oviducts is decreased in vitro by exposure to solutions of mainstream and sidestream cigarette smoke. *Biol Reprod* 53(1):29–37
26. Lehnert BE, Lyster R (2002) Exposure to low-level chemicals and ionizing radiation: reactive oxygen species and cellular pathways. *Hum Environ Toxicol* 21:65–69
27. Li F, Zhou X, Wong STC (2010) Optimal live cell tracking for cell cycle study using time-lapse fluorescent microscopy images. *Mach Learn Med Imaging* 6357:124–131
28. Lin S, Talbot P (2010) Methods for culturing mouse and human embryonic stem cells. *Embryonic stem cell therapy for osteodegenerative disease*. Humana Press, New York, pp 31–56
29. Lin S, Talbot P (2014) Stem cells. In: Wexler P (ed) *The encyclopedia of toxicology*, 3rd edn. Elsevier (in press)
30. Lin S, Tran V, Talbot P (2009) Comparison of toxicity of smoke from traditional and harm-reduction cigarettes using mouse embryonic stem cells as a novel model for preimplantation development. *Hum Reprod* 24(2):386–397
31. Lin S, Fonteno S, Satish S, Bhanu B, Talbot P (2010) Video bioinformatics analysis of human embryonic stem cell colony growth. *J Vis Exp*. <http://www.jove.com/index/details.stp?id=1933>
32. Lin S, Fonteno Shawn, Weng Jo-Hao, Talbot P (2010) Comparison of the toxicity of smoke from conventional and harm reduction cigarettes using human embryonic stem cells. *Toxicol Sci* 118:202–212
33. Martin GG, Talbot P (1981) The role of follicular smooth muscle cells in hamster ovulation. *J Exp Zool* 216(3):469–482
34. Reichen M, Veraichm FS, Szita N (2010) An automated and multiplexed microfluidic bioreactor platform with time-lapse imaging for cultivation of embryonic stem cells and on-line assessment of morphology and pluripotent markers. In: 14th international conference on miniaturized systems for chemistry and life sciences, Groningen, The Netherlands
35. Riveles K, Iv M, Arey J, Talbot P (2003) Pyridines in cigarette smoke inhibit hamster oviductal functioning in picomolar doses. *Reprod Toxicol* 17(2):191–202
36. Riveles K, Roza R, Arey J, Talbot P (2004) Pyrazine derivatives in cigarette smoke inhibit hamster oviductal functioning. *Reprod Biol Endocrinol* 2(1):23
37. Riveles K, Roza R, Talbot P (2005) Phenols, quinolines, indoles, benzene, and 2-cyclopenten-1-ones are oviductal toxicants in cigarette smoke. *Toxicol Sci* 86(1):141–151



38. Riveles K, Tran V, Roza R, Kwan D, Talbot P (2007) Smoke from traditional commercial, harm reduction and research brand cigarettes impairs oviductal functioning in hamsters (*Mesocricetus auratus*) in vitro. *Hum Reprod* 22(2):346–355
39. Schatten G (1981) The movements and fusion of the pronuclei at fertilization of the sea urchin *Lytechinus variegates*: time-lapse video microscopy. *J Morphol* 167:231–247
40. Talbot P (1983) Videotape analysis of hamster ovulation in vitro. *J Exp Zool* 225(1):141–148
41. Talbot P, Lin S (2010) Cigarette smoke's effect on fertilization and pre-implantation development: assessment using animal models, clinical data, and stem cells. *J Biol Res* 44:189–194
42. Talbot P, Lin S (2010) Mouse and human embryonic stem cells: can they improve human health by preventing disease? *Curr Topics Med Chem* 11:1638–1652. (PMID 21446909)
43. Talbot P, Geiske C, Knoll M (1999) Oocyte pickup by the mammalian oviduct. *Mol Biol Cell* 10(1):5–8
44. Talbot P, zur Nieden N, Lin S, Martinez I, Guan B, Bhanu B (2014) Use of video bioinformatics tools in stem cell toxicology. *Handbook of Nanomedicine, Nanotoxicology and Stem Cell Use in Toxicology* (in press)
45. Thannickal VJ, Fanburg BL (2000) Reactive oxygen species in cell signaling. *Am J Physiol Lung Cell Mol Physiol* 279:L1005–L1028
46. Tsai KL, Talbot P (1993) Video microscopic analysis of ionophore induced acrosome reactions of lobster (*Homarus Americanus*) sperm. *Mol Reprod Dev* 36(4):454–461
47. Valavanidis A, Vlachogianni T, Fiotakis K (2009) Tobacco smoke: involvement of reactive oxygen species and stable free radicals in mechanisms of oxidative damage, carcinogenesis and synergistic effects with other respirable particles. *Int J Environ Res Public Health* 6(2):445–462
48. Wang Y, Moussavi F, Lorenzen P (2013) Automated embryo stage classification in time-lapse microscopy video of early human embryo development. *Lect Notes Comput Sci* 8150:460–467
49. Weng JH, Phandthong G, Talbot P (2014) A video bioinformatics method to quantify cell spreading and its application to cells treated with rho associated protein kinase and blebbistatin. In: Bhanu B, Talbot P (eds) *Video bioinformatics*. Springer, Berlin
50. Williams M, Villarreal A, Bozhilov K, Lin S, Talbot P (2013) Metal and silicate particles including nanoparticles are present in electronic cigarette cartomizer fluid and aerosol. *PLoS One* 8(3):e57987. doi:[10.1371/journal.pone.005798](https://doi.org/10.1371/journal.pone.005798)
51. Wong CC, Loewke KE, Bossert NL, Behr B, De Jonge CJ, Baer TM, Reijo-Pera RA (2010) Non-invasive imaging of human embryos before embryonic genome activation predicts development to the blastocyst stage. *Nat Biotechnol* 28:1115–1121

Author Query Form

Book ID : **315486_1_En**
Chapter No.: **9**



Please ensure you fill out your response to the queries raised below and return this form along with your corrections

Dear Author

During the process of typesetting your chapter, the following queries have arisen. Please check your typeset proof carefully against the queries listed below and mark the necessary changes either directly on the proof/online grid or in the 'Author's response' area provided below

Query Refs.	Details Required	Author's Response
AQ1	No queries.	

MARKED PROOF

Please correct and return this set

Please use the proof correction marks shown below for all alterations and corrections. If you wish to return your proof by fax you should ensure that all amendments are written clearly in dark ink and are made well within the page margins.

<i>Instruction to printer</i>	<i>Textual mark</i>	<i>Marginal mark</i>
Leave unchanged	... under matter to remain	Ⓟ
Insert in text the matter indicated in the margin	⧵	New matter followed by ⧵ or ⧵ [Ⓢ]
Delete	/ through single character, rule or underline or ⎓ through all characters to be deleted	⧻ or ⧻ [Ⓢ]
Substitute character or substitute part of one or more word(s)	/ through letter or ⎓ through characters	new character / or new characters /
Change to italics	— under matter to be changed	↵
Change to capitals	≡ under matter to be changed	≡
Change to small capitals	≡ under matter to be changed	≡
Change to bold type	~ under matter to be changed	~
Change to bold italic	≈ under matter to be changed	≈
Change to lower case	Encircle matter to be changed	≡
Change italic to upright type	(As above)	⧻
Change bold to non-bold type	(As above)	⧻
Insert 'superior' character	/ through character or ⧵ where required	Y or Y under character e.g. Y or Y
Insert 'inferior' character	(As above)	⧵ over character e.g. ⧵
Insert full stop	(As above)	⊙
Insert comma	(As above)	,
Insert single quotation marks	(As above)	Y or Y and/or Y or Y
Insert double quotation marks	(As above)	Y or Y and/or Y or Y
Insert hyphen	(As above)	⎓
Start new paragraph	⌞	⌞
No new paragraph	⌞	⌞
Transpose	⌞	⌞
Close up	linking ○ characters	⌞
Insert or substitute space between characters or words	/ through character or ⧵ where required	Y
Reduce space between characters or words		↑